INL/CON-06-01375
PREPRINT

Hydrogen Production From Nuclear Energy Via High Temperature Electrolysis

1st Energy Center Hydrogen Initiative Symposium

James E. O'Brien
Carl M. Stoots
J. Stephen Herring
Grant L. Hawkes

April 2006

The INL is a
U.S. Department of Energy
National Laboratory
operated by
Battelle Energy Alliance

The 1st Energy Center Hydrogen Initiative Symposium, Purdue University,
West Lafayette, IN 47907, USA, April 5-6, 2006.

Paper: ECHI-I-IL-3

HYDROGEN PRODUCTION FROM NUCLEAR ENERGY VIA HIGH TEMPERATURE ELECTROLYSIS

James E. O'Brien[1], Carl M. Stoots, J. Stephen Herring, Grant L. Hawkes
Idaho National Laboratory, Idaho Falls, ID 83415
james.obrien@inl.gov

ABSTRACT

This paper presents the technical case for high-temperature nuclear hydrogen production. A general thermodynamic analysis of hydrogen production based on high-temperature thermal water splitting processes is presented. Specific details of hydrogen production based on high-temperature electrolysis are also provided, including results of recent experiments performed at the Idaho National Laboratory. Based on these results, high-temperature electrolysis appears to be a promising technology for efficient large-scale hydrogen production.

KEYWORDS

Nuclear hydrogen, high-temperature electrolysis.

1. INTRODUCTION

There is a growing interest in the development of large-scale non-fossil hydrogen production technologies. This interest is driven by the immediate demand for hydrogen for refining of increasingly low-quality petroleum resources (e.g., the Athabasca oil sands), the expected intermediate-term demand for carbon-neutral synthetic fuels, and the possible long-term demand for carbon-free hydrogen as an environmentally benign transportation fuel. Large-scale efficient carbon-free hydrogen production can be accomplished by water splitting based on nuclear energy. Two candidate technologies are under consideration: thermochemical processes and high-temperature electrolysis. A schematic of these candidate nuclear hydrogen production technologies is provided in Fig. 1. Note that the primary energy input for thermochemical processes is in the form of heat, whereas the primary energy input for high-temperature electrolysis is in the form of electricity. Thermochemical processes comprise a series of thermally driven chemical reactions which have the net effect of water splitting with hydrogen and oxygen as products. The other reactants are recycled during the process. The most studied thermochemical process for nuclear hydrogen production is the sulfur-iodine (SI) process (Brown et al., 2003). The sulfuric acid decomposition reaction in the SI process requires heat addition at a temperature of approximately 900°C. Active research activities on the SI process are under way in the US and in Japan. Primary challenges include corrosion, catalyst degradation, and membranes separations. High-temperature electrolysis utilizes a combination of thermal energy and electricity to split water in solid-oxide electrolysis cells (SOECs). These cells are very similar to solid-oxide fuel cells (SOFCs). The feasibility of operating solid-oxide cells at high

[1] Corresponding author

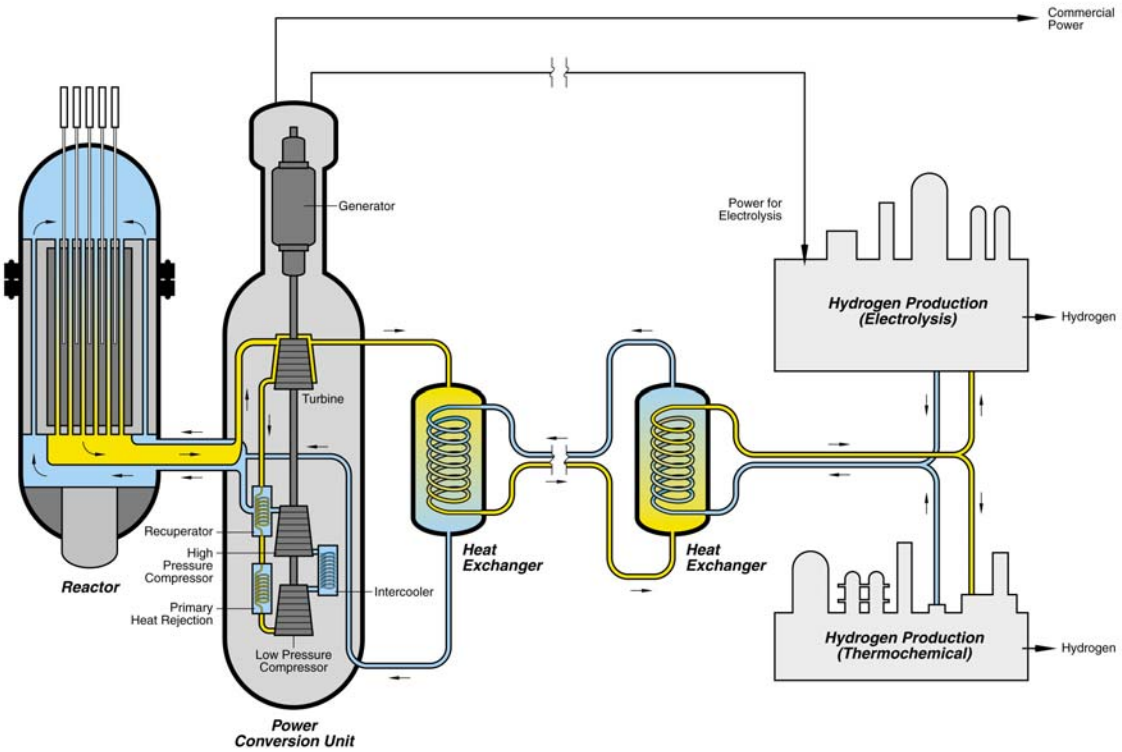

Figure 1. Nuclear hydrogen production concepts: thermochemical process and high-temperature electrolysis.

temperature in the electrolysis mode has been demonstrated for both tubular (Maskalick, 1986) and planar systems (O'Brien et al., 2005). System modeling studies have been performed to compare the predicted overall hydrogen-production efficiency of the SI process with high-temperature electrolysis (Yildiz and Kazimi, 2003). Results of these studies indicate similar expected performance for the two methods. However, high-temperature electrolysis faces fewer technical challenges to large-scale deployment.

2. THERMODYNAMICS OF THERMAL WATER SPLITTING

A basic thermodynamic analysis can be applied to a general thermal water-splitting process, as shown in Fig. 2, in order to determine the overall process efficiency limits as a function of temperature. Water enters the control volume from the left. Since the ultimate feedstock for any large-scale water-splitting operation will be liquid water, it is reasonable to consider the case in which water enters the control volume in the liquid phase at temperature T and pressure P. Pure hydrogen and oxygen streams exit the control volume on the right, also at T and P. Two heat reservoirs are available, one at temperature T_H and one at temperature T_L. Heat transfer between these reservoirs and the control volume is indicated in the figure as Q_H and Q_L. Note that there is no work crossing the control-volume boundary. Therefore if the process under consideration is high-temperature electrolysis, both the power cycle and the electrolyzer are located inside the control volume.

From a chemical reaction standpoint, the water-splitting process corresponds to the dissociation or reduction of water:

$$H_2O \rightarrow H_2 + \tfrac{1}{2}\, O_2 \qquad (1)$$

The first and second laws of thermodynamics can be applied to this process as follows:

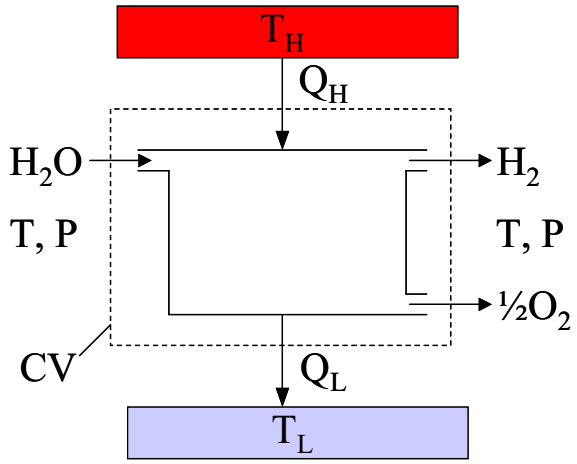

Figure 2. Schematic of a thermal water-splitting process operating between temperatures T_H and T_L.

1st law:
$$Q_H - Q_L = \Delta H_R \tag{2}$$

2nd law:
$$\Delta S_R \geq \frac{Q_H}{T_H} - \frac{Q_L}{T_L} \tag{3}$$

where ΔH_R is the enthalpy of reaction and ΔS_R is the entropy change of the reaction. The overall thermal-to-hydrogen efficiency of thermal water splitting processes can be defined in terms of the net enthalpy change of the working fluid (can also be thought of as the energy content or heating value of the produced hydrogen), divided by the (costly) high-temperature heat added to the system:

$$\eta_H = \frac{\Delta H_R}{Q_H} \tag{4}$$

Combining the first and second law equations for the reversible case and substituting into the efficiency definition yields:

$$\eta_{H,\max} = \frac{1 - T_L / T_H}{1 - T_L \Delta S_R / \Delta H_R} \tag{5}$$

Note that the water splitting process defined in Fig. 2 is simply the reverse of the combustion of hydrogen with oxygen. Therefore the enthalpy of reaction for the water-splitting process is the opposite of the enthalpy of combustion, which by definition is equal to the "heating value" of the hydrogen. Since for our process, we have assumed that the water enters the control volume in the liquid phase,

$$\Delta H_R = HHV \tag{6}$$

where HHV is the "high heating value" of hydrogen. If we further assume that T and P represent standard conditions, and that $T_L = T_o$,

$$\Delta H_R - T_L \Delta S_R = -\Delta G^o_{f,H_2O} \tag{7}$$

such that the efficiency expression can be rewritten as:

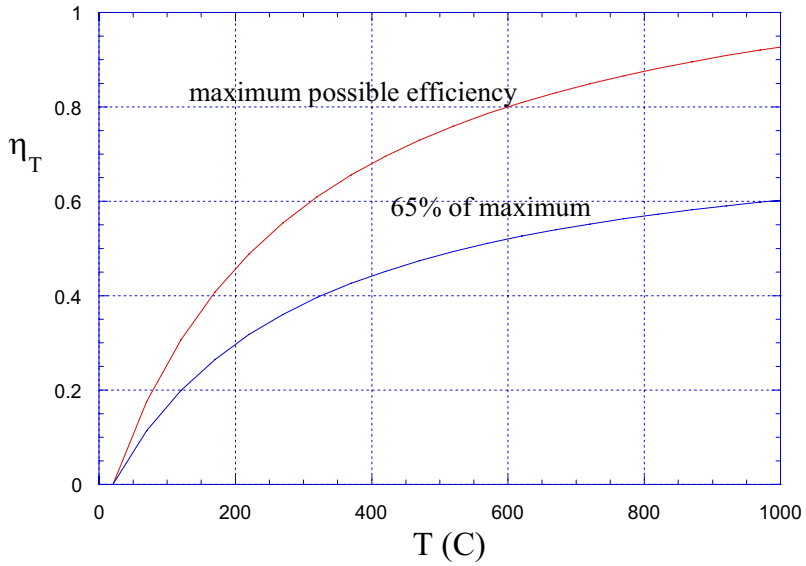

Figure 3. Theoretical thermal water splitting efficiencies.

$$\eta_{H,\max} = \left(1 - \frac{T_L}{T_H}\right)\left(\frac{HHV}{-\Delta G^o_{f,H_2O}}\right) = \left(1 - \frac{T_L}{T_H}\right)\left(\frac{1}{0.83}\right) \tag{8}$$

The high heating value of the hydrogen and the standard-state Gibbs energy of formation for water are fixed quantities such that the second factor on the right-hand side is a constant.

A plot of this result is presented in Fig. 3 for T_L = 20°C. The top curve represents the maximum possible water-splitting efficiency result given by Eqn. (8). The bottom curve is simply 65% of this thermodynamic limit. The 65% value is based on a typical percentage of Carnot efficiency that can be achieved with a well engineered modern power cycle. The first conclusion to be drawn is that high temperature is needed for efficient thermal-water-splitting-based hydrogen production, independent of the method used. If we assume that 65% of the maximum possible efficiency might also be achievable with a well engineered thermal water-splitting process, then efficiencies of the magnitude given in the lower curve of Fig. 3 should be expected. Detailed system analyses performed at MIT (Yildiz and Kazimi, 2003) have shown that both HTE and the Sulfur-Iodine (SI) thermochemical processes should be able to achieve overall thermal-to-hydrogen efficiencies greater than 55% at a temperature of 950°C. Their analysis also shows a much steeper drop-off in performance with lower heat addition temperatures for the SI process than for HTE. Coolant outlet temperatures for advanced high-temperature reactors are now expected to be lower than 900°C, which favors HTE.

3. THERMODYNAMICS OF HIGH TEMPERATURE ELECTROLYSIS

Focusing now on high-temperature electrolysis, the solid oxide electrolysis cell is a solid-state electrochemical device consisting of an oxygen-ion-conducting electrolyte (e.g., yttria-stabilized zirconia, YSZ) with porous electrically conducting electrodes deposited on either side of the electrolyte. As shown in Fig. 4, a mixture of steam and hydrogen at 750-950°C is supplied to the cathode side of the electrolyte. The oxygen ions are drawn through the electrolyte by the applied electrochemical potential, liberating their electrons and recombining to form molecular O_2 on the anode side. The entering steam-hydrogen mixture may be as much as 90% steam. Similarly, the exiting mixture may be as much as 90% H_2. The product steam and hydrogen gas mixture is passed through a condenser or membrane separator to purify

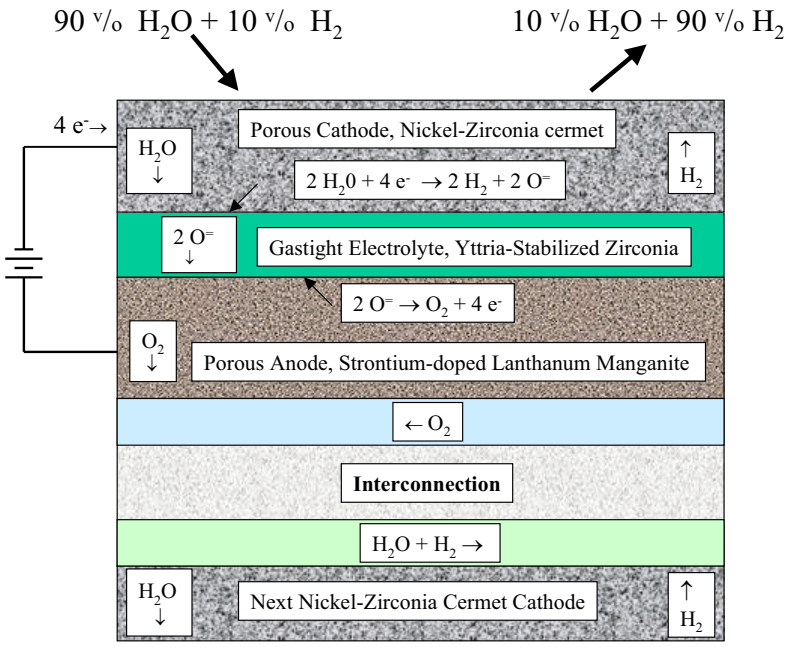

Figure 4. Components of a High Temperature Electrolysis Cell.

the hydrogen. The electrolytic cells are combined to form a stack, separated by electronically conducting interconnects.

Operation of a solid-oxide stack in the electrolysis mode is fundamentally different than operation in the fuel-cell mode for several reasons, aside from the obvious change in direction of the electrochemical reaction. From the standpoint of heat transfer, operation in the fuel-cell mode typically necessitates the use of significant excess air flow in order to prevent overheating of the stack. The potential for overheating arises from two sources: (1) the exothermic nature of the hydrogen oxidation reaction, and (2) the ohmic heating associated with the electrolyte ionic resistance and other loss mechanisms.

Conversely, in the electrolysis mode, the steam reduction reaction is endothermic. Therefore, depending on the current density, the net heat generation in the stack may be negative, zero, or positive. This phenomenon is illustrated in Fig. 5. The figure shows the respective internal heat source fluxes in a planar solid-oxide stack associated with the electrochemical reaction and the ohmic heating. The net heat flux is also shown. A stack-average area-specific resistance of 1.25, an operating temperature of 1200 K, and hydrogen mole fractions of 0.1 and 0.95 at the inlet and outlet, respectively, were assumed for these calculations. The net heat flux is always positive and increases rapidly with current density in the fuel-cell mode. In the electrolysis mode, the net heat flux is negative at low current densities, increasing to zero at the "thermal-neutral" voltage, and positive at higher current densities. The thermal-neutral voltage can be predicted from direct application of the First Law to the overall system:

$$\dot{Q} - \dot{W} = \Delta\dot{N}_{H_2} \Delta H_R \tag{9}$$

where

$$\Delta\dot{N}_{H_2} = I / 2F \tag{10}$$

Letting $Q = 0$ (no external heat transfer), $\dot{W} = IV_{tn}$,

$$V_{tn} = \Delta H_R / 2F \tag{11}$$

Since the enthalpy of reaction, ΔH_R, is strictly a function of temperature, the thermal-neutral voltage is also strictly a function of temperature, independent of cell *ASR* and gas compositions. The particular values of net cell heat flux at other operating voltages do however depend on cell *ASR* and gas

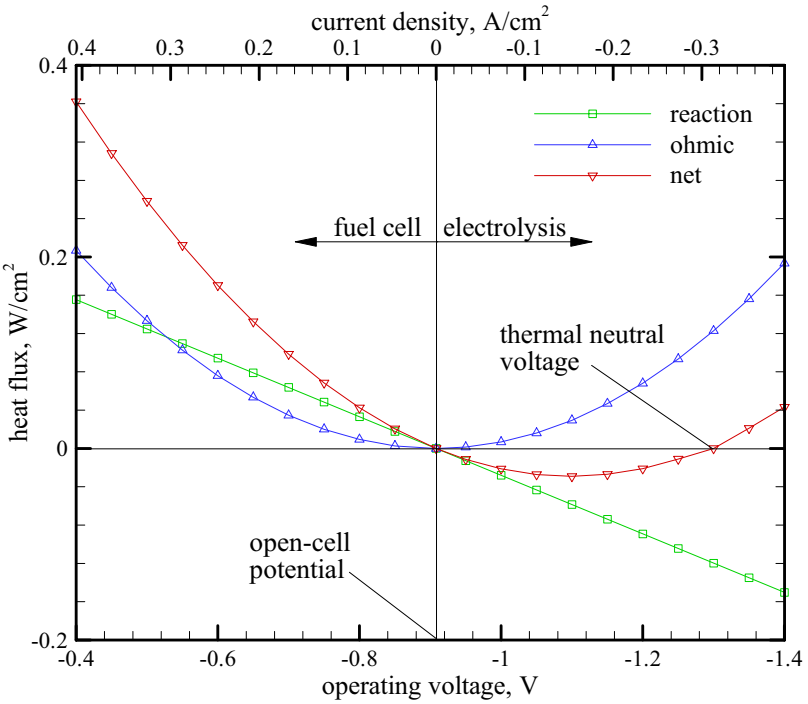

Figure 5. Thermal contributions in electrolysis and fuel cell modes of operation.

compositions. The thermal-neutral voltage increases only slightly in magnitude over the typical operating temperature range for solid-oxide cells, from 1.287 V at 800°C to 1.292 V at 1000°C. At typical solid-oxide electrolysis stack temperatures and *ASR* values, operation at the thermal-neutral voltage yields current densities in the 0.2 – 0.4 A/cm^2 range, which is very close to the current density range that has yielded successful long-term operation in of solid-oxide fuel cell stacks. Operation at or near the thermal-neutral voltage simplifies thermal management of the stack since no significant excess gas flow is required. In fact, in the electrolysis mode, since oxygen is being produced, there is also no theoretical need for air flow to support the reaction at all. In a large-scale electrolysis plant, the pure oxygen produced by the process could be saved as a valuable commodity. However, there are several good reasons to consider the use of a sweep gas on the oxygen side. First, the use of a sweep gas will minimize the performance degradation associated with any small leakage of hydrogen from the steam/hydrogen side to the oxygen side of the cell. Second, there are serious materials issues associated with the handling of pure oxygen at elevated temperatures. Finally, the use of a sweep gas (especially one that does not contain oxygen) on the oxygen side of the electrolysis cell reduces the average mole fraction of oxygen, thereby reducing the open-cell and operating potentials, resulting in higher electrolysis efficiencies, according to Eqn. (13).

Electrolysis efficiency, η_e, can be defined for HTE, analogous to the definition of fuel cell efficiency (e.g., Laramie and Dicks, 2003). The electrolysis efficiency quantifies the heating value of the hydrogen produced by electrolysis per unit of electrical energy consumed in the stack. Based on this definition,

$$\eta_e = \frac{\dot{N}_{H_2} \Delta H_R}{VI} \tag{12}$$

and since the stack electrical current is directly related to the molar production rate of hydrogen via Faraday's law, the electrolysis efficiency can be expressed strictly in terms of cell operating potentials as:

$$\eta_e = \frac{\Delta H_R / 2F}{V_{op}} = \frac{V_{tn}}{V_{op}}. \tag{13}$$

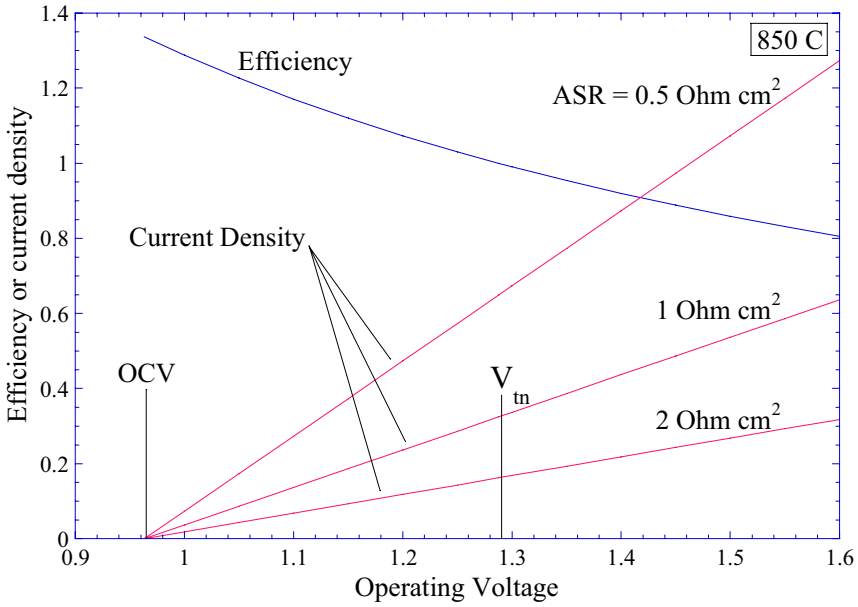

Figure 6. Effect of operating voltage and area-specific resistance on electrolysis

The efficiency for the fuel-cell mode of operation is the inverse of Eqn. (13).

It should be noted that the value of the efficiency defined in this manner for electrolysis is generally greater than 1.0. As an example, for the reversible reference case, the cell potential approaches the open-cell value, $E_o = \Delta G_R / 2F$, yielding:

$$\eta_{e,o} = \frac{\Delta H_R}{\Delta G_R} \tag{14}$$

which for steam electrolysis at 850ºC is equal to 1.34. For cases with variable gas composition, the open-cell potential is given by the Nernst Equation:

$$E_{ocv} = E_o - \frac{R_u T}{jF} \ln\left[\left(\frac{y_{H2O}}{y_{H2} y_{O2}^{1/2}}\right)\left(\frac{P}{P_{std}}\right)^{-1/2}\right] \tag{15}$$

and the corresponding efficiency limit varies accordingly. It is not desirable to operate an electrolysis stack near the efficiency limit, however, because the only way to approach this limit is to operate with very low current density. There is a trade-off between efficiency and hydrogen production rate in selecting an electrolysis stack operating voltage. This trade-off is illustrated in Fig. 6. The upper curve in the figure shows the decrease in electrolysis efficiency that occurs as the per-cell operating voltage is increased above the open-cell voltage (OCV), according to Eqn. (13). Operation at the thermal-neutral voltage yields an electrolysis efficiency of 1.0. Area-specific resistance (*ASR*) represents the net effect of all the loss mechanisms in the electrolysis stack including, ohmic losses, activation and concentration overpotentials, etc. The bottom curves show the effect of operating voltage and *ASR* on the current density. Noting that:

$$i = \frac{V_{op} - E_{ocv}}{ASR}, \tag{16}$$

if a target current density (and corresponding hydrogen production rate) is selected, lower *ASR* values allow for stack operation at lower voltages and correspondingly higher efficiencies. Similarly, in the fuel-cell mode, there is a tradeoff between efficiency and maximum power production. Maximum power

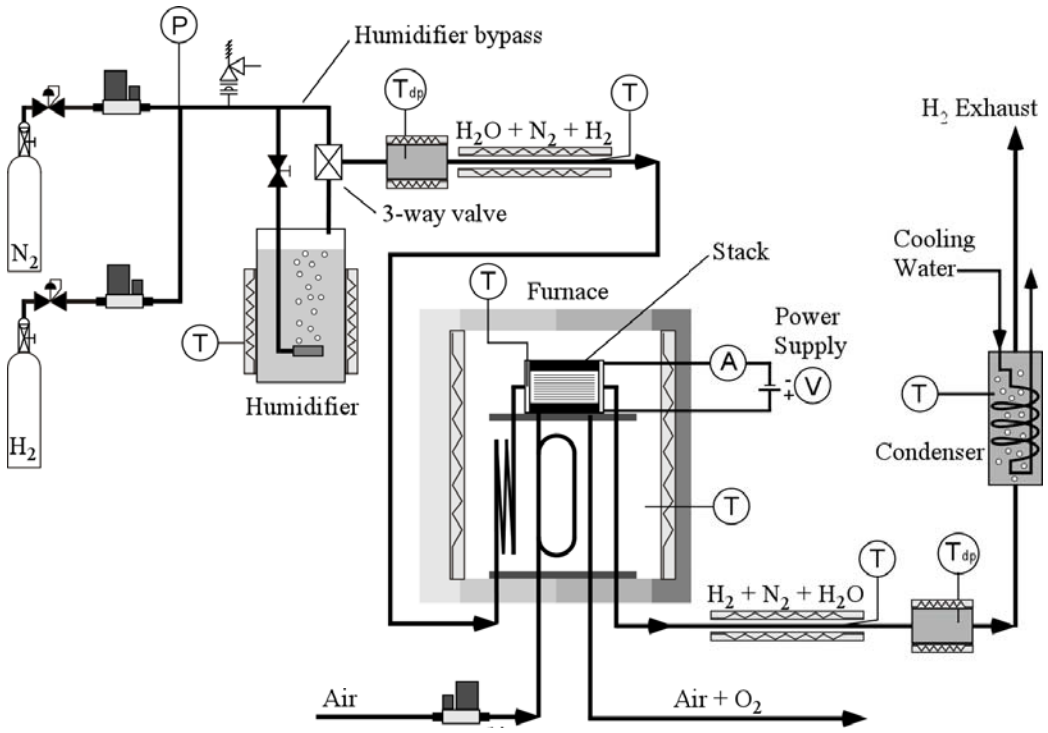

Figure 7: Schematic of experimental apparatus for electrolysis stack testing.

production for solid-oxide fuel cells occurs for operation at around 0.5 V, whereas maximum efficiency occurs at the open-cell potential, around 0.9 V. Depending on optimization parameters, a good operating point usually occurs at around 0.7 V in the fuel-cell mode of operation. In the electrolysis mode, a good tradeoff between efficiency and hydrogen will occur at operating voltages below $\Delta H_R/2F$, around 1.1 V. The challenge is to develop SOEC stacks with low *ASR* such that a reasonable current density will be achievable at this low operating voltage.

4. HIGH-TEMPERATURE ELECTROLYSIS EXPERIMENTS

Recent test results obtained with a 25-cell HTE stack illustrate some of the concepts discussed in this paper. HTE stack tests are performed using the apparatus shown schematically in Fig. 7. The HTE stack is located in a large furnace operated at 800 - 850°C. The stack is fed a steam/hydrogen/nitrogen mixture that flows on top of each cell and air on the bottom of each cell in cross flow. Electrolysis yields a steam/hydrogen/nitrogen outlet stream that is enriched in hydrogen and an air outlet stream that is enriched in oxygen. Independent measurement of the steam consumption rate is provided by inlet and outlet dewpoint measurements. Additional details of the apparatus can be obtained from references (O'Brien et al., 2005).

Electrolysis stack performance can be evaluated by performing DC potential sweeps for each stack in order to characterize its performance over a range of operating conditions. Each sweep is performed in the electrolysis mode with the furnace temperature and gas flow rates set at fixed values, but with the power supply programmed to vary the applied voltage over a range, typically from 0.8 to 1.5 volts/cell. Results of these sweeps are useful for obtaining information about cell *ASR* values and steam starvation limits.

Results of two representative sweeps obtained with a 25-cell stack are shown in Fig. 8 in the form of polarization curves, representing per-cell operating voltage versus current density. Test conditions for each of the two sweeps are tabulated in the figure. Sweep 25-1 was obtained soon after the stack was initially heated to 800°C. This sweep was performed in a stepwise fashion, rather than as a continuous sweep. This was done in order to ensure sufficient time for the internal stack temperatures to achieve steady-state values at each operating voltage. Note that the slope of sweep 25-1 is low, indicating a low

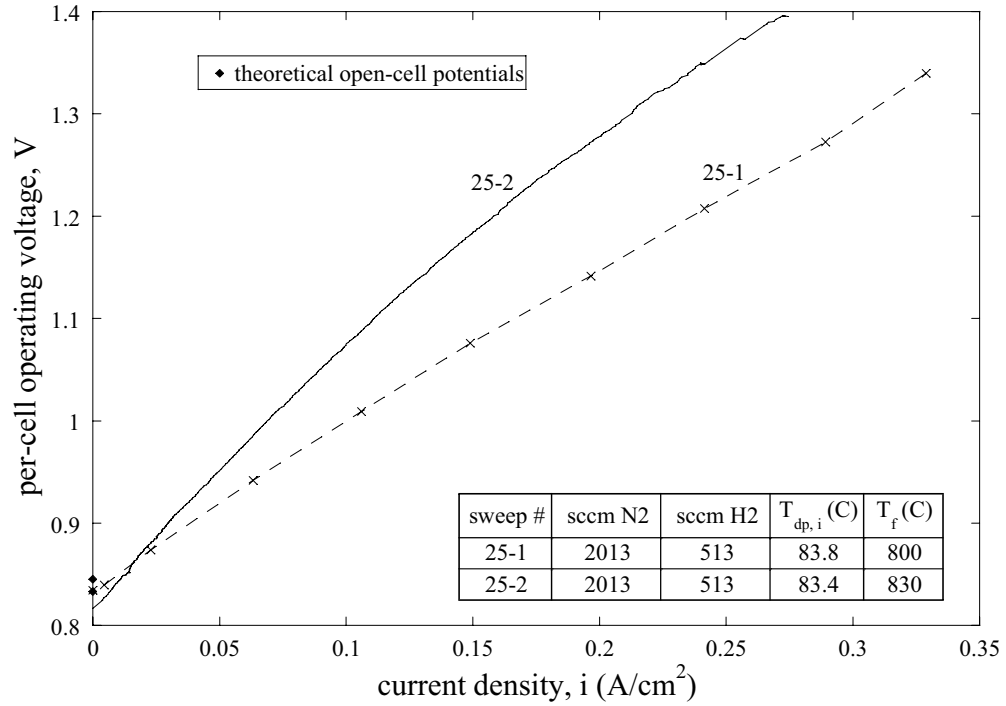

Figure 8. Polarization curves for 25-cell stack.

ASR value around 1.5 Ohm·cm^2. Sweep 25-2 was acquired in a continuous fashion at the end of the long-duration test. The stack operating temperature was increased from 800°C to 830°C part way through the test. Note that the slope of the final sweep is lower than that of the initial sweep, despite the higher temperature, due to performance degradation over 1000 hours of operation.

Hydrogen production rates during a DC potential sweep can be calculated directly from the stack electric current (Eqn. 10) and independently from the measured inlet and outlet dewpoint measurements.

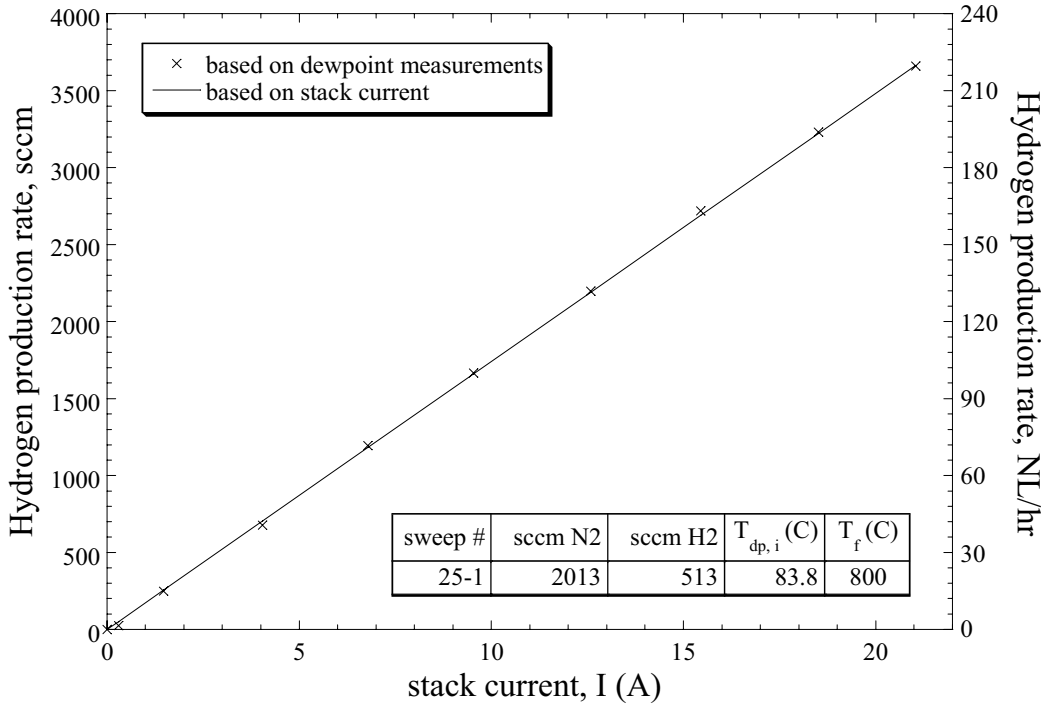

Figure 9. Hydrogen production rates during DC potential sweep.

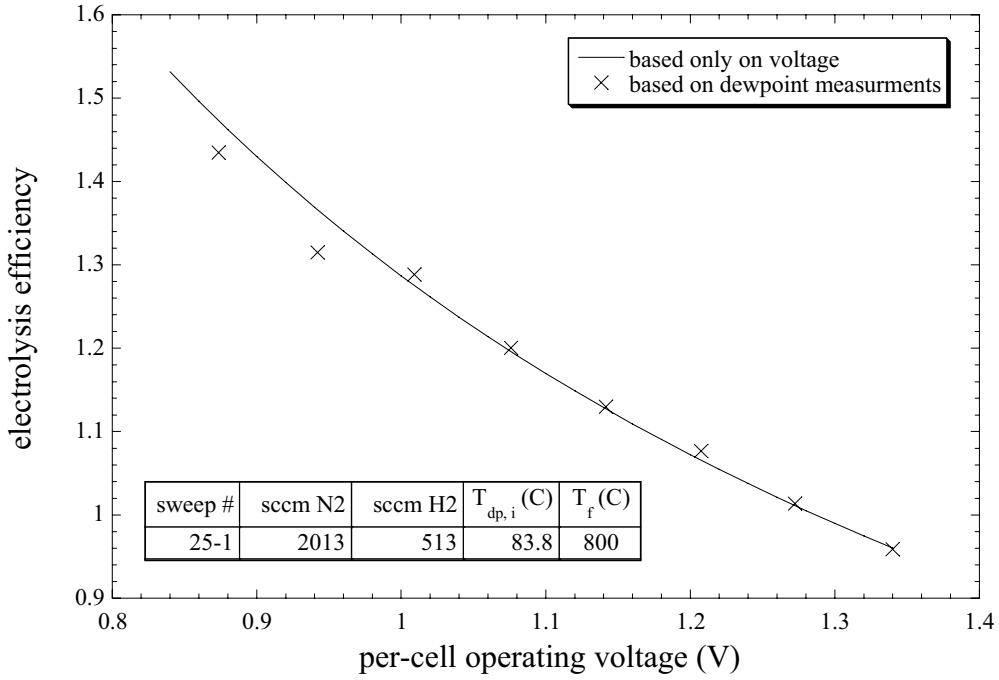

Figure 10. Electrolysis efficiencies as a function of operating voltage.

A representative plot of hydrogen production rates measured during the stepwise sweep 25-1 is shown in Fig. 9. The left-hand vertical scale is in standard cubic centimeters per minute (sccm) and the right-hand vertical axis is in normal liters per hour (NL/hr). The current-based hydrogen production rate is simply a straight line since hydrogen production is directly proportional to the stack current. The dewpoint-based measurements exhibit excellent agreement with the current-based measurements. Hydrogen production rates as high as 220 NL/hr were achieved with this stack.

Electrolysis efficiencies corresponding to the hydrogen production rates shown in Fig. 9 are presented in Fig. 10 as a function of stack operating voltage. Efficiency values based on stack operating voltage and values based on the measured change in dewpoint temperatures, the corresponding hydrogen production rates, and measured stack voltage and current are shown (see Eqns. 12 and 13). These independent efficiency measurements are in excellent agreement. Electrolysis efficiency decreases monotonically with increasing stack operating voltage. The efficiency is a maximum at the open-cell potential and it is equal to 1.0 at the thermal neutral voltage (1.287 V at 800ºC). Electrolysis operation is a tradeoff between maximum efficiency and hydrogen production rate. Low stack ASR values allow for achievement of a specified hydrogen production rate (or current density) at lower operating voltages and correspondingly higher electrolysis efficiencies.

Internal stack temperatures measured during a DC potential sweep are presented in Fig. 11 as a function of operating voltage at a furnace temperature of 800°C. These temperature measurements were obtained using miniature thermocouples inserted to a depth of 5 cm into the air flow channels of the 25-cell stack. Stack internal thermocouple T_1 was located in the center air flow channel, halfway between the midpoint and the steam/hydrogen inlet. Stack internal thermocouple T_2 was inserted into the center position of the fifth cell from the bottom of the stack. The internal stack thermocouples respond as expected during the sweep. At voltages between the open-cell potential and the thermal neutral voltage, in the electrolysis mode, the stack internal temperatures are lower than the gas inlet and furnace setpoint temperatures because at these operating voltages, the endothermic reaction heat requirement is greater than the ohmic heating (Fig.5) and there is a net cooling effect on the stack. A thermal minimum point is reached at an operating voltage that is halfway between the open-cell voltage and the thermal-neutral voltage (~1.06 V in Fig. 11) and full thermal recovery is observed near the thermal neutral voltage of 1.29 V/cell. The magnitude of the stack cooling and heating effects is greatest at the center of the stack. We have predicted similar internal stack temperature trends using a three-dimensional computational fluid

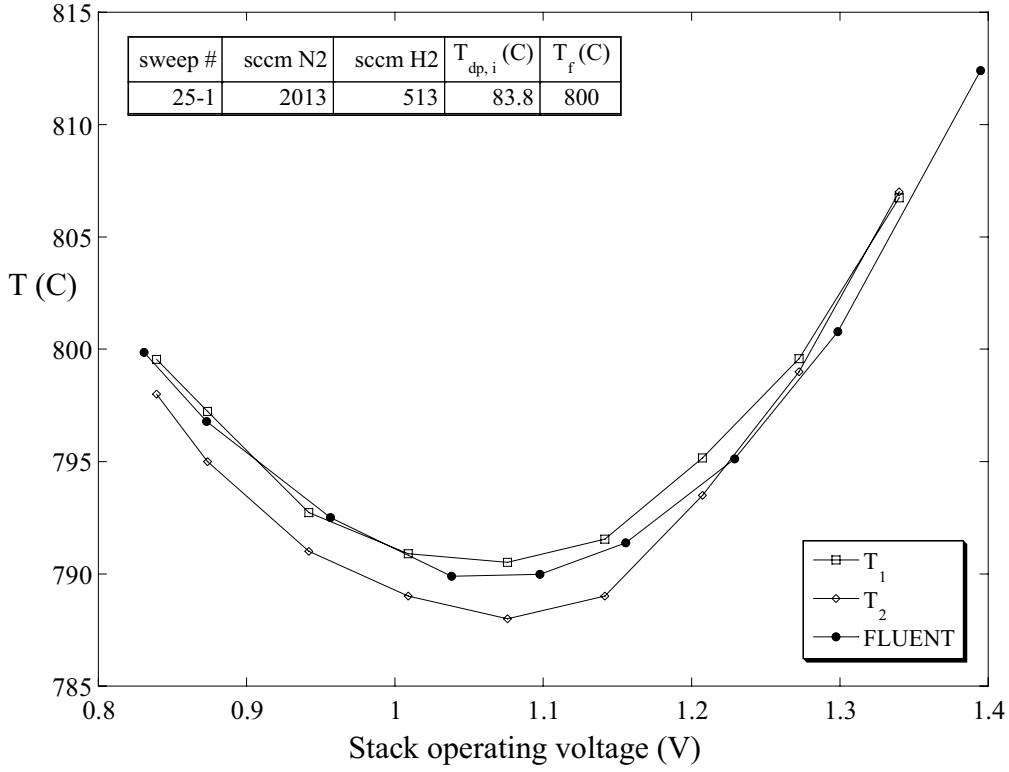

Figure 11. Stack temperatures measured during DC potential sweep.

dynamic (CFD) model of a planar electrolysis cell (Hawkes et al., 2005). The CFD model replicates the geometry of a single cell as it exists in a stack. It was created using *FLUENT* with an SOFC user-defined subroutine, operating in the electrolysis mode. The SOFC module handles the electrochemical reactions, loss mechanisms, electric field computation, and electrode porous-media constitutive relations (Prinkey et al., 2004). This reference also documents the treatment of species and energy sources and sinks arising from the electrochemistry at the electrode-electrolyte interfaces. Mean electrolyte temperatures predicted from our *FLUENT* CFD model under corresponding operating conditions are also presented in Fig. 11. The CFD model includes a radiant boundary condition around the periphery of the cell to simulate the furnace environment. The agreement between the measured internal stack temperatures and the CFD model predictions is excellent.

5. CONCLUSIONS

Large-scale efficient carbon-free hydrogen production can be accomplished by water splitting based on nuclear energy. Based on a thermodynamic analysis of a general thermal water-splitting process, high-temperature operation is required to achieve high efficiency. This conclusion is a primary driver for the development of high-temperature advanced reactor systems. Furthermore, system analyses have shown that high-temperature electrolysis efficiencies should be comparable to those of the thermochemical processes at operating temperatures near 900°C. Operation in the electrolysis mode minimizes thermal management issues since the electrolysis reaction is endothermic. Electrolysis efficiency is shown to be inversely proportional to the operating voltage. Therefore low cell area-specific resistance is desirable to allow a reasonable hydrogen production rate with a low operating voltage. Experimental results obtained with a 25-cell electrolysis stack reveal the performance trends associated with operation over a range of operating voltages and current densities. The stack exhibited an average ASR value of 1.5 Ohm·cm^2. Internal stack temperature measurements and CFD predictions show a stack cooling effect for operating voltages below thermal neutral.

NOMENCLATURE

ASR	area-specific resistance, Ohm cm^2
E_o	standard open-cell potential, V
E_{OCV}	Nernst or open-cell potential, V
F	Faraday number, J/V/mol
ΔG_f^o	standard-sate Gibbs energy of formation, J/mol
ΔG_R	Gibbs energy of reaction, J/mol
ΔH_R	enthalpy of reaction, J/mol
HHV	high heating value, J/mol
i	current density, A/cm^2
I	current, A
j	moles of electrons transferred per mole of steam electolyzed
$\dot{N}$	molar flow rate, mol/s
$\Delta\dot{N}$	molar production or consumption rate, mol/s
P	pressure, kPa
P_{std}	standard-state pressure, kPa
Q_H	heat transfer at high temperature, J/mol
Q_L	heat transfer at low temperature, J/mol
$\dot{Q}$	heat transfer rate, W
R_u	universal gas constant, J/mol/K
ΔS_R	entropy of reaction, J/mol
T	temperature, K
V_{tn}	thermal-neutral voltage, V
V_{op}	operating voltage, V
$\dot{W}$	power, W
y	mole fraction
η_H	thermal water splitting efficiency
η_e	electrolysis efficiency

ACKNOWLEDGEMENTS

This work was funded by the US Department of Energy, Office of Nuclear Energy, under the Nuclear Hydrogen Initiative. The Idaho National Laboratory is operated by the Battelle Energy Alliance for the Department of Energy.

REFERENCES

Brown, L. C., Lentsch, R. D., Besenbruch, G. E., Schultz, K. R., "Alternative Flowsheets for the Sulfur-Iodine Thermochemical Hydrogen Cycle," *AIChE Journal,* April 2003.

Brown, L. C., Besenbruch, G. E., Lentsch, R. D., Schultz, K. R., Funk, J. F., Pickard, P. S., Marshall, A. C., Showalter S. K., "High Efficiency Generation of Hydrogen Fuels Using Nuclear Power – Final Technical Report for the Period August 1, 1999 through September 30, 2002", Prepared under the Nuclear Energy Research Initiative (NERI) Program Grant No. DE-FG03-99SF21888 for the U.S. Department of Energy, June 2003.

Hawkes, G. L., O'Brien, J. E., Stoots, C. M., Herring, J. S., Shahnam, M., "Thermal and Electrochemical Three Dimensional CFD Model of a Planar Solid Oxide Electrolysis Cell," Proceedings, 2005 ASME Heat Transfer Conference, July 17-22, 2005, San Francisco.

Larminie, J. and Dicks, A., *Fuel Cell Systems Explained*, John Wiley & Sons, New York, 2003.

Maskalick, N. J., "High Temperature Electrolysis Cell Performance Characterization," Int. J. Hydrogen Energy, pp. 563-570, 1986.

O'Brien, J. E., Stoots, C. M., Herring, J. S., Lessing, P. A., Hartvigsen, J. J., and Elangovan, S., "Performance Measurements of Solid-Oxide Electrolysis Cells for Hydrogen Production from Nuclear Energy," *Journal of Fuel Cell Science and Technology*, Vol. 2, August 2005, pp. 156-163.

O'Brien, J. E., Stoots, C. M., Herring, J. S., and Hartvigsen, J. J.,"Hydrogen Production Performance of a 10-Cell Planar Solid-Oxide Electrolysis Stack," Proceedings, ASME 3rd International Conference on Fuel Cell Science, Engineering, and Technology, May 23 – 25, 2005, Ypsilanti, MI.

Prinkey, M., Shahnam, M., and Rogers, W. A., "SOFC FLUENT Model Theory Guide and User Manual," Release Version 1.0, FLUENT, Inc., 2004.

Yildiz, B., and Kazimi, M. S., "Nuclear Energy Options for Hydrogen and Hydrogen-Based Liquid Fuels Production," MIT-NES-TR-001, September 2003.